

https://doi.org/10.1070/QEL16992

Acceleration of electrons in the interaction of a subterawatt laser pulse with a nonuniform plasma

V.S. Popov, N.E. Andreev

Abstract. **We consider the effect of nonlinear self-focusing and self-modulation processes on the acceleration of electrons in the interaction of a subterawatt femtosecond laser pulse with a gas jet plasma. A three-dimensional particle-in-cell (3D PIC) simulation of the interaction of laser radiation with a low-density nonuniform plasma shows that laser pulse self-focusing that arises when the critical power of relativistic self-focusing determined by the local concentration of plasma electrons exceeds the pulse power results in efficient generation of a plasma wave. Due to a decrease in the phase velocity of the wake plasma wave generated via self-modulation of the laser pulse, electrons are trapped into the accelerating phase of the plasma wave and are accelerated to energies of ~10 MeV. It is demonstrated that under the conditions for limiting the electrons' acceleration region by the length of their dephasing, quasi-monoenergetic electron bunches with a characteristic energy of ~9 MeV can be produced. The effective temperature of the accelerated electrons and their angular distribution, obtained by 3D PIC simulation, are in good agreement with those determined in the experiment.**

Keywords: *electron acceleration, subterawatt laser pulse, nonuniform plasma, relativistic self-focusing.*

1. Introduction

Recently, significant results have been achieved in the laser-plasma acceleration of electrons. In 2014, a quasi-monoenergetic electron beam with a record energy of 4.2 GeV was generated at the Lawrence Berkeley National Laboratory using a 0.3-PW BELLA laser with a pulse energy of ~30 J [1]. On the other hand, for many applications, such as ultra-fast low-dose radiography, materials research, production of isotopes, etc., other sources of electrons of relatively low energies, 10–20 MeV, are required; to reach such low energies, the laser pulse energy can be relatively small, i.e. ~0.1 J. Lasers with such parameters are found in many laboratories. Sources of quasi-monoenergetic electrons with energies of tens of MeV can also serve as injectors for the subsequent acceleration of electrons in laser-plasma accelerating cascades to high energies (tens and hundreds of GeV). In this regard, the development of a compact laser-plasma electron accelerator with a sub-terawatt power driver is a promising direction.

V.S. Popov, N.E. Andreev Joint Institute for High Temperatures, Russian Academy of Sciences, ul. Izhorskaya 13, stroenie 2, 125412 Moscow, Russia; Moscow Institute of Physics and Technology (State University), Institutskii per. 9, 141700 Dolgoprudnyi, Moscow region; e-mail: andreev@ras.ru, nikolay.e.andreev@gmail.com

Received 6 March 2019
Kvantovaya Elektronika **49** (4) 307–313 (2019)
Translated by I.A. Ulitkin

The first studies of the acceleration of electrons by a subterawatt laser pulse demonstrated the possibility of accelerating electron bunches with a fairly small charge (~10 fC) using a 10 mJ laser in a thin (~100 μm) jet of argon or helium [2]. Goers et al. [3] produced electron bunches with an exponential energy distribution and energy up to 10–12 MeV. The authors of this work note that the relativistic effect of laser pulse self-focusing plays a significant role in the process of electron trapping and acceleration.

The generation of high-energy electron beams by focusing a laser pulse with an energy of 100 mJ on the edge of a solid target was studied in [4, 5]. The effect of ionisation effects on the propagation of a laser pulse, its self-modulation, generation of wake fields and electron acceleration in an aluminium plasma is considered in [6].

In the present work, using the three-dimensional particle-in-cell (3D PIC) simulation, we examine the mechanisms of trapping and accelerating an electron bunch by taking into account nonlinear self-focusing and self-modulation [7] of subterawatt laser pulse during its interaction with a nonuniform gas jet plasma. The energy and angular characteristics of accelerated electrons are investigated and the energy spectrum of electrons is compared with that obtained experimentally [3].

2. Simulation parameters

Figure 1 shows the schematic of the numerical simulation. The calculation parameters of the laser pulse incident on the plasma corresponded to the experimental conditions [3]. The FWHM duration τ_{las} of a Gaussian laser pulse, which propagates along the x axis, was equal to 50 fs. The laser pulse energy was $W = 40$ mJ, which corresponded to the laser pulse power $P = W/\tau_{las} = 0.8$ TW. The pulse was linearly polarised along the y axis and had a Gaussian shape with an FWHM diameter d_{FWHM} of 9.7 μm. The laser wavelength was $\lambda = 1$ μm. The dimensionless field amplitude at the maximum was $a_0 = eE_0/(m_e c\omega_0) = 0.72$, where e is the absolute value of the electron charge; m_e is the electron mass; c is the speed of light; and ω_0 is the laser frequency. This amplitude corresponds to the intensity $I_0 = 7 \times 10^{17}$ W cm^{-2}.

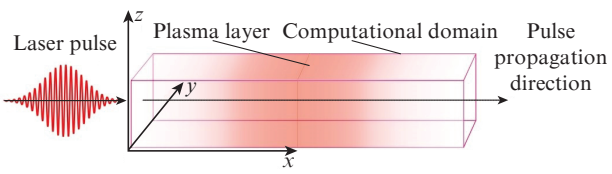

Figure 1. Schematic of numerical calculation.

The length of the computational domain along the laser pulse propagation direction (x axis) was equal to 600 μm, and the transverse size in both directions (y and z) was 60 μm. The hydrogen plasma had a nonuniform Gaussian density profile in the direction of the x axis and a uniform distribution in the transverse direction (Fig. 2):

$$n_e(x) = n_0 \exp[-(x - x_c)^2/l^2] \text{ with } |x - x_c| \leqslant d, \quad (1)$$

where $x_c = 300$ μm is the centre of the region; $l = 120$ μm; and $d = 240$ μm. At the edges of the region ($|x - x_c| > d$), the Gaussian profile (1) was supplemented with a more rapidly decreasing function with a continuous derivative at the sewing point to reduce the simulation domain at close-to-zero density values at the boundaries:

$$n_e(x) = n_0 \exp[-(x - x_c)^2/l^2]\exp[-(|x - x_c| - d)^2/b^2]$$
$$\text{with } |x - x_c| > d, \quad (2)$$

where $b = 25$ μm.

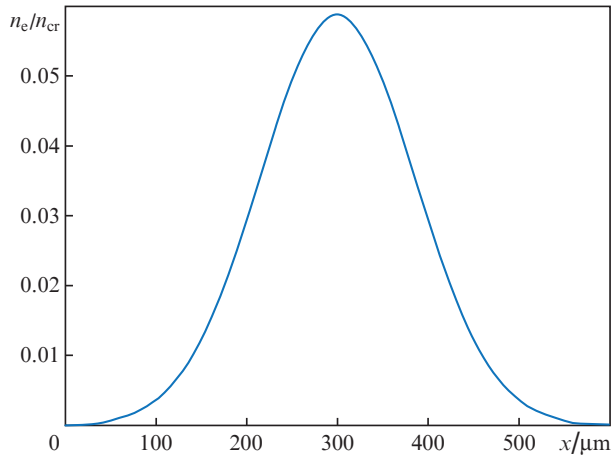

Figure 2. Example of the initial Gaussian profile of the plasma electron concentration along the laser pulse propagation direction, used in the calculations.

The calculations were performed using the three-dimensional relativistic particle-in-cell code VLPL [8] for two values of the maximum electron concentration in the centre of the region, $n_0 = 0.059n_{cr}$ and $n_0 = 0.19n_{cr}$, which corresponds to 6.5×10^{19} cm^{-3} and 2.1×10^{20} cm^{-3}, where $n_{cr} = m_e\omega_0^2/(4\pi e^2)$ is the critical plasma concentration, equal to 1.1×10^{21} cm^{-3} for the wavelength $\lambda = 1$ μm.

The size of the computational cell was $0.05 \times 0.5 \times 0.5$ μm along the x, y and z axes, respectively. The time step was $c\Delta t = 0.048$ μm. The number of particles in the computational cell was equal to 4 for $n_0 = 0.059n_{cr}$ and 16 for $n_0 = 0.19n_{cr}$. This number of particles per cell is necessary to obtain high-energy electrons (from 7 MeV) in an amount sufficient to construct correct angular distributions of particles in this energy range. At the initial instant of time, the plasma was considered cold, that is, $T_e = T_i = 0$.

3. Dynamics of laser pulse self-focusing

For the concentration $n_0 = 0.059n_{cr}$, Fig. 3 presents the dependences of the maximum on-axis field amplitude and the width of the laser beam (FWHM) on its propagation time. The dashed curve shows the initial distribution of the electron concentration (in arbitrary units), and the dot-dashed lines shows the region of self-focusing. The process of laser pulse self-focusing leads to a significant increase in the intensity of the laser field and a decrease in its characteristic width. With the beginning of self-focusing ($ct \approx 180$ μm), the on-axis amplitude of the laser field begins to grow dramatically from $a = eE_y/(m_e c\omega_0) = 0.6$ and reaches a maximum of $a = 1.6$ at $ct = 380$ μm. At the same time, the width of the laser pulse reaches a minimum ($d_{FWHM} = 3.4$ μm).

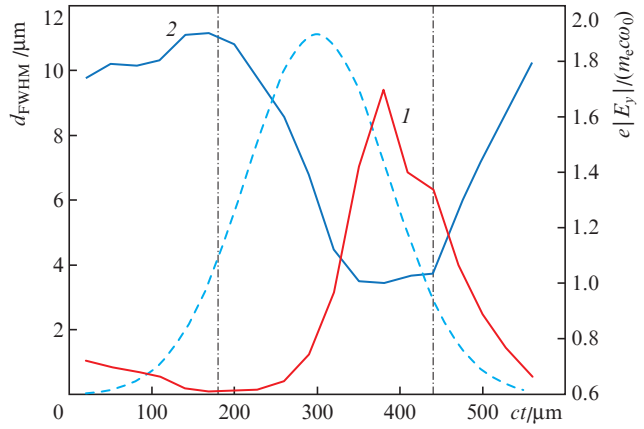

Figure 3. Time dependences of (*1*) the maximum value of the laser field on the axis and (*2*) the FWHM width of the laser beam. Vertical dash-dotted lines indicate the region of self-focusing. The dashed line shows the initial distribution of the electron concentration in arbitrary units in the region where the maximum of the laser pulse is located at a given time.

The self-focusing process begins when the laser pulse propagating through a plasma with an increasing concentration reaches a region in which the laser pulse power approaches the critical power of relativistic self-focusing. The plasma concentration at which self-focusing begins is $n_e/n_{cr} = 0.018$. This concentration corresponds to the critical pulse power, $P_{cr} = 17.4n_{cr}/n_e = 956$ GW. Thus, the ratio of the laser pulse power to the critical power in this region is $P/P_{cr} = 0.84$.

Since, with only transverse compression of a pulse, its amplitude will increase proportionally to a decrease in its width, the 3.2-fold pulse compression (Fig. 3) should correspond to a 3.2-fold increase in the laser field. However, the laser field increases only 2.67 times, which also indicates a change in the longitudinal pulse shape, leading to a three-dimensional redistribution of its energy.

4. Dynamics of laser pulse self-modulation and wake wave excitation

Owing to the self-focusing of a laser pulse, its wave front steeping and self-modulation instability, a wake plasma wave is efficiently generated [9]. The plasma wave field on the x axis (along the laser pulse propagation direction) can be estimated in the approximation quadratic in laser pulse amplitude using the expression [10]:

$$E_x(\xi) = -(m_e c^2/e)(k_p^2/4)\int_{\infty}^{\xi} d\xi' |a(\xi', t)|^2 \cos[k_p(\xi - \xi')]. \quad (3)$$

Here, $k_p = \omega_p/v_g$ is the wave vector of the plasma wave; $\omega_p^2 = 4\pi n_e e^2/m_e$ is the plasma frequency; $v_g \cong c$ is the group velocity of the laser pulse; $a(\xi, t)$ is the normalised value of the laser pulse envelope on the axis; and $\xi = x - ct$.

Figures 4 and 5 show for $ct = 290$ and 380 μm (correspond to the period of developed self-focusing of the pulse, see Fig. 3) the x-axis distributions of the unperturbed electron concentration, laser pulse envelope E_y and wake plasma wave field E_x, obtained by numerical simulation and the wake wave field (3), determined by the calculated envelope of the laser pulse.

Figures 4b and 4c show the spatial distributions of the laser pulse envelope and the wake wave for $ct = 290$ μm, corresponding to the beginning of the pulse self-modulation process (Fig. 6). In this case, the modulation of the laser pulse envelope is weakly expressed, the amplitude of the excited wake wave is small, and the plasma wave is well described over the first few periods by the linearised expression (3).

The dependences at $ct = 380$ μm, shown in Fig. 5, correspond to a strongly developed regimes of laser pulse self-modulation and self-focusing (Figs 3, 5b and 6). In this highly nonlinear regime, the laser pulse field exceeds the relativistic value, $eEy/(m_e c\omega_0) > 1$, but formula (3) allows the structure

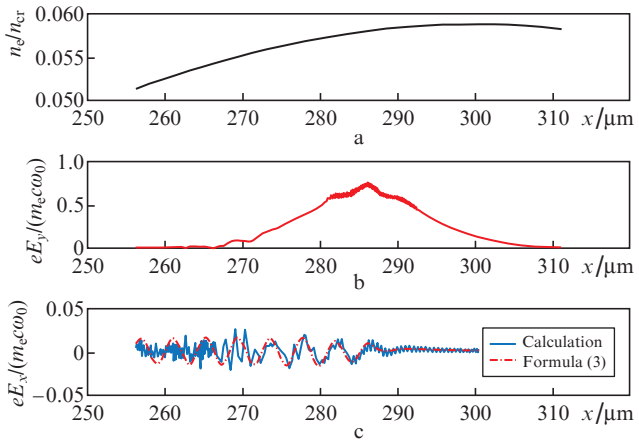

Figure 4. Distributions of (a) the unperturbed electron concentration, (b) laser pulse envelope E_y and (c) wake plasma wave field E_x along the x axis, obtained by numerical simulation, and the wake wave field (3) determined by the laser pulse envelope [(c), dash-dotted curve] at $ct = 290$ μm.

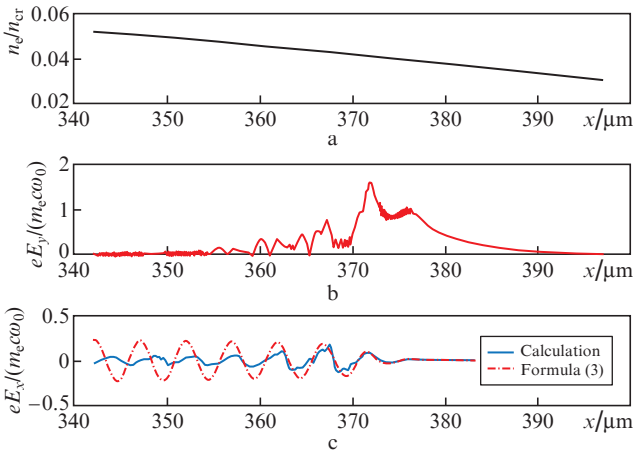

Figure 5. Same as in Fig. 4, but at $ct = 380$ μm.

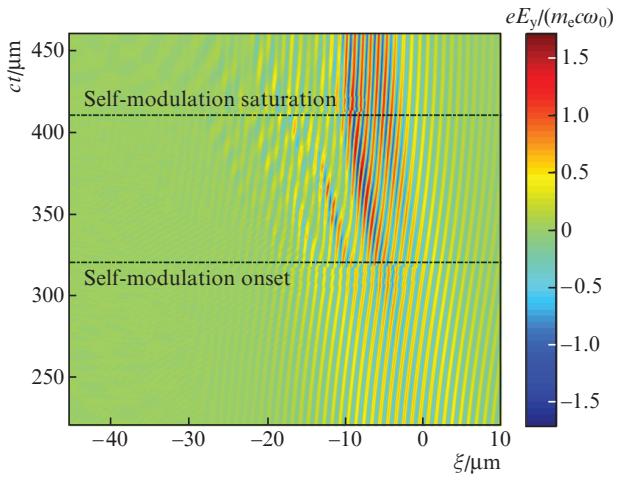

Figure 6. (Colour online) Dependences of the laser pulse field distribution on the axis in the coordinates ct and ξ. The horizontal lines mark the times of the laser pulse self-modulation onset and saturation.

and amplitude of the plasma wave to be estimated with an accuracy of ~ 10% in the first period of the excited wake field.

In addition to the plasma wave amplitude, the phase velocity of this wave also plays an important role in the process of trapping of background plasma electrons. Its decrease in comparison with the group velocity of a laser pulse contributes to the effective trapping and acceleration of electrons. The phase velocity of a plasma wave decreases with the development of self-modulation instability [11], as well as due to linear effects of the laser pulse propagation in a nonuniform density plasma and a change in the length of the plasma wave generated by it. Figure 7 shows the on-axis distribution of the wake plasma wave field in the coordinates ct and ξ at $ct = 260$–460 μm. Black lines indicate the trajectories of the values of the constant wave phase. The slope of these lines, which determines the phase velocity of the wave, means a decrease in the phase velocity for all periods of the excited wave at $ct > 320$ μm. At the same time, the phase velocity of the wake wave moving away from the leading edge of the laser pulse ($\xi = x - ct \cong 2$ μm at $ct = 260$ μm), where the generation of the wake field begins, decreases compared to the laser-pulse group velocity that is close to the speed of light.

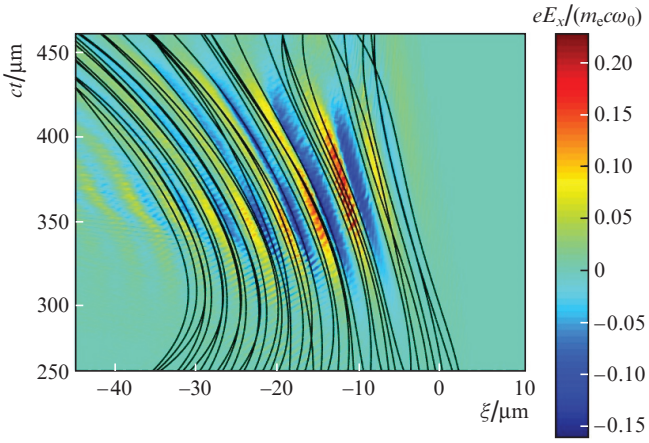

Figure 7. (Colour online) Dependences of the field distribution of the wake plasma wave on the axis in the coordinates ct and ξ. The black lines are the trajectories of the values of the constant phase of the wave.

The background electrons are trapped in the regions of the maxima of the accelerating wake wave field (minima of the negative value of the field E_x normalised using the absolute value of the electron charge e, Fig. 7). The wake wave phase velocity in these regions is determined by both the velocity of the main maximum of the laser pulse, followed by the predominant generation of the accelerating field, and by the distance (wake wave period number) from the generation region (maximum of the laser pulse), see Figs 6 and 7. Figure 8 shows the velocity of the main maximum of the laser pulse in the range of 280–440 μm, and also gives an estimate of the laser-pulse group velocity using a linear dispersion equation for a nonuniform plasma [$v_g/c = \sqrt{1 - n_e(x)/n_{cr}}$, where n_e is the unperturbed electron concentration]. With the beginning of the laser pulse self-modulation process ($ct > 320$ μm, see Fig. 6), one can clearly see a decrease in the velocity of the main maximum of the laser pulse as a result of this nonlinear process, which is significantly less than the linear estimate of the laser-pulse group velocity in a nonuniform plasma and determines in the region of generation (Fig. 9, the solid curve for $n = 1$).

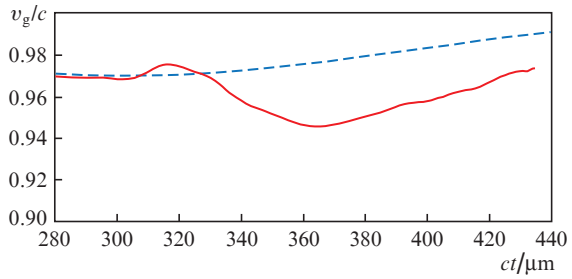

Figure 8. Velocity of the main maximum of the laser pulse (solid curve), and the estimate of the group velocity of the laser pulse using the linear dispersion equation in a nonuniform plasma (dashed line).

Figure 9 displays the change in the wake wave phase velocity for the five maxima of the accelerating field (the minima of the negative value of the field E_x), following the laser pulse maximum. The dashed curves for the same five values of the wake wave phase show how the phase velocity changes as a result of linear changes in the laser-pulse group velocity and the length of a wake wave in a nonuniform plasma. Different curves correspond to the velocities of different maxima of the accelerating field in five periods of the plasma wave ($n = 1–5$), measured from the main maximum of the laser pulse amplitude, followed predominantly by the wake wave generation. The phase velocity in the linear approximation was stimated under the assumption that the leading edge of the plasma wave moves with the group velocity of the laser pulse, which is determined by the linear dispersion equation, and other parts of the plasma wave in this approximation move at a velocity determined with a constant phase velocity proportional to the integral:

$$\int_{ct+\xi(ct)}^{ct+\xi_{fr}(ct)} \sqrt{n_e(x)/n_{cr}}\,dx$$

[ξ_{fr} is the accompanying coordinate of the laser pulse maximum; $\xi(ct)$ is the accompanying coordinate of the constant phase; and $n_e(x)$ is the unperturbed density of electrons at point x].

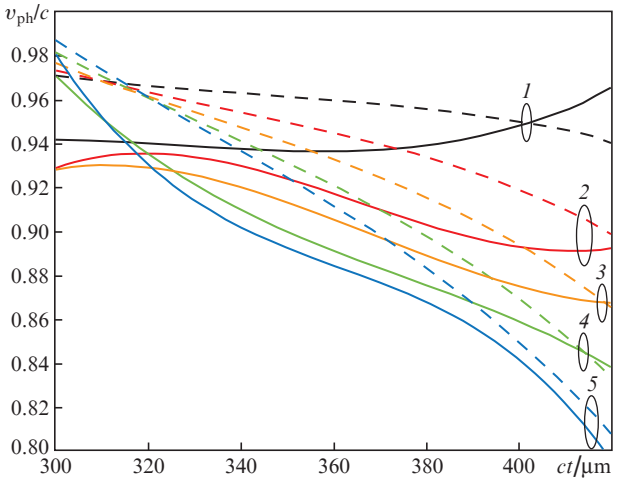

Figure 9. (Colour online) Change in the wake wave phase velocity v_{ph} with time for different maxima of the accelerating field ($n = 1–5$), following the main maximum of the laser field (solid curves), as well as an estimate of the phase velocity based on linear effects caused by nonuniform plasma concentrations (dashed curves).

As shown in Fig. 10, the background electrons are trapped at $ct \approx 350$ μm in the second and subsequent periods of the wake wave ($n = 2–5$). It follows from Fig. 9 that in the whole interval, from $ct \approx 350$ μm (when electrons are being trapped) to $ct \approx 380$ μm (when accelerated electrons with maximum energy enter the decelerating phase of the wake wave, see Fig. 11), the values of the phase velocities obtained from the self-consistent calculation for all maxima of the accelerating field at which the electron are trapped are substantially less than the values obtained according to a linear estimate of the effect of plasma nonuniformity. This indicates a significant contribution of nonlinear effects to a decrease in phase velocity, which is important for trapping background plasma electrons. The linear effect of plasma nonuniformity, which is insignificant in the region of the maximum of the unperturbed plasma concentration ($x \approx 300$ μm), also makes a significant contribution to a decrease in the wake wave phase velocity with increasing distance of the laser pulse from the maximum of the unperturbed plasma concentration and with increasing distance from the generation region (see the

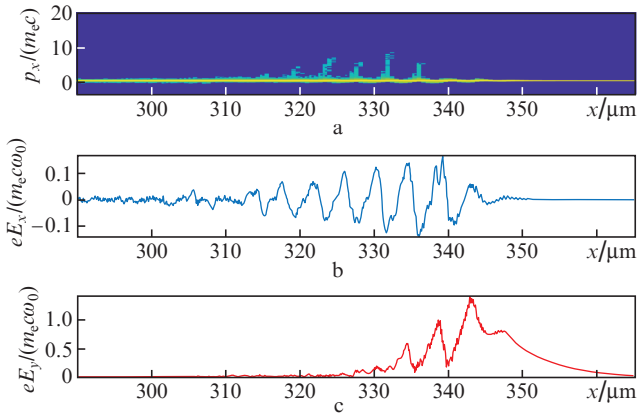

Figure 10. (a) Phase plane (x, P_x) of the plasma electrons, (b) spatial distribution of the plasma wave field, and (c) laser pulse amplitude on the x axis for $ct = 350$ μm and $n_0 = 0.059 n_{cr}$.

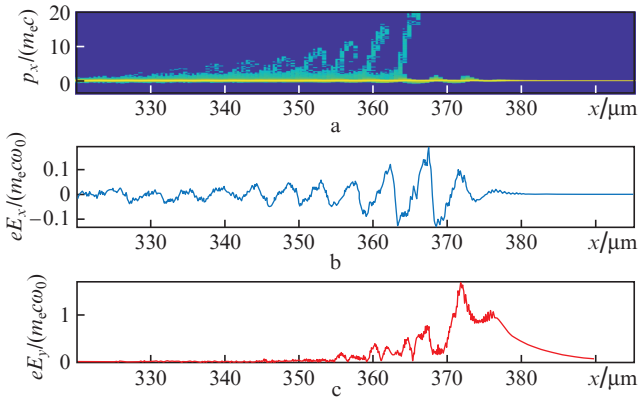

Figure 11. Same as in Fig. 10, but at $ct = 380$ μm.

dashed curves in Fig. 9). Note that at $ct > 380$ μm, when the influence of nonlinear effects weakens (laser pulse self-modulation is saturated), the wake wave phase velocity, according to a linear estimate, for periods located sufficiently far from the leading front of its generation approaches the phase velocity obtained in self-consistent calculation (see curves for $n = 5$ in Fig. 9).

5. Electron trapping and acceleration

Starting from the instant of time corresponding to $ct \approx 350$ μm, when the amplitude of the laser pulse field reaches a maximum during self-focusing (see Fig. 3), and the development of the pulse self-modulation leads to an efficient wake wave generation (see Figs 6 and 7), background plasma electrons begin to be trapped by the wake plasma wave field (Fig. 10a), which is produced mainly behind the main maximum of the laser pulse (Figs 10b and 10c).

The process of acceleration of trapped electrons continues until the accelerated electrons, keeping ahead of the wake wave, enter the decelerating phase of the wave (Fig. 11). In this case, electrons are grouped in the phase space, which is reflected in the formation of 'quasi-monoenergetic' bunches (a 'hillock on the tail' with a characteristic energy of ~9 MeV) in the energy spectrum of accelerated electrons (Fig. 12). The characteristic temperature T_e of electrons with an energy of less than 7 MeV is 5.2 MeV.

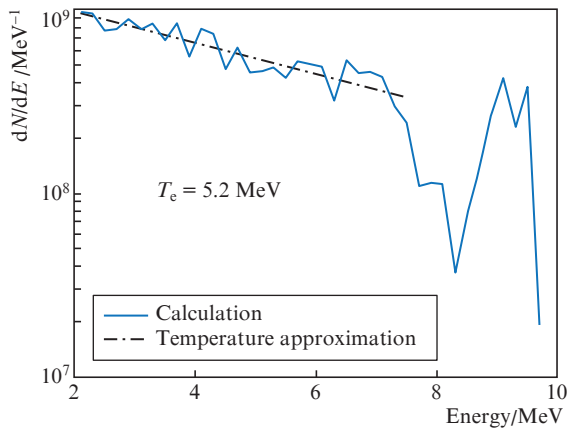

Figure 12. Spectrum of accelerated electrons at $ct = 380$ μm and $n_0 = 0.059 n_{cr}$.

With the electrons moving further in the field of the wake wave that gradually attenuates as the plasma concentration decreases, the electrons are mixed in phase space and a 'temperature' distribution is formed in the entire energy range of accelerated electrons (Fig. 13).

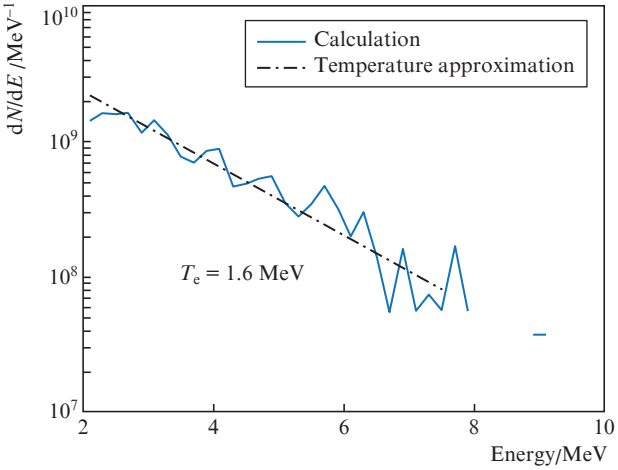

Figure 13. Spectrum of accelerated electrons emitted from the plasma during the entire interaction time ($ct > 550$ μm) at $n_0 = 0.059 n_{cr}$.

Most of the electrons, entering the braking phase of the plasma wave, lose their energy, and the number of low-energy electrons (2–3 MeV) increases two-three times (cf. Figs 11 and 12). In this case, the characteristic temperature of electrons decreases and becomes equal to 1.6 MeV. The absence of electrons in certain ranges for energy above 8 MeV in Fig. 13 is a consequence of the small number of particles used in this calculation.

To compare the simulation results with the data obtained in experiment [3], the calculation was performed for the maximum electron concentration $n_0 = 0.19 n_{cr}$, which corresponds to 2.1×10^{20} cm^{-3}. The energy spectrum of the accelerated electrons emitted from the target during the entire interaction time is shown in Figs 14 and 15. A decrease in the characteristic temperature and a corresponding decrease in the number

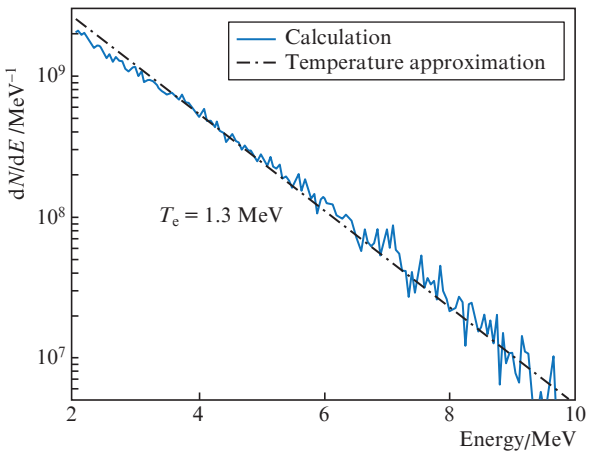

Figure 14. Energy spectrum of electrons emitted from the plasma at $n_0 = 0.19 n_{cr}$.

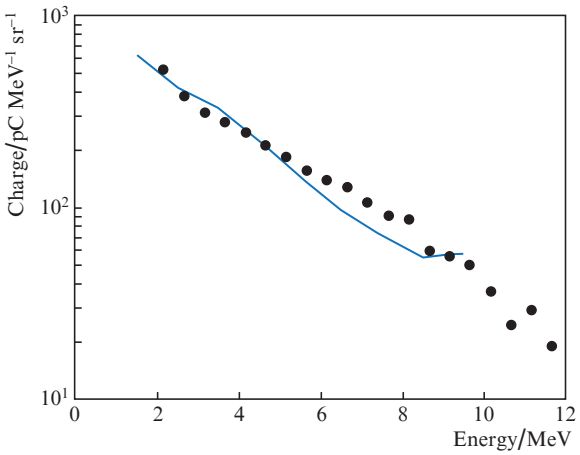

Figure 15. Energy spectra of electrons emitted from a plasma, obtained (solid curve) from PIC simulations and (points) in the experiment [3], normalised to the solid angle into which electrons fly at $n_0 = 0.19n_{cr}$. The calculated spectrum is multiplied by 3.63.

of accelerated electrons in the 'tail' of the distribution (at energies above 5 MeV) with increasing plasma concentration (cf. Figs 13 and 14) is due to a decrease in the wake wave phase velocity and the dephasing length determined by it, during which electrons gain energy.

The energy spectrum in Fig. 15 is normalised to the magnitude of the solid angle, into which electrons fly, for each energy range. The normalisation was carried out taking into account the widths of the angular distributions of electrons over the polar and azimuth angles. Figure 16 shows the angular distributions of a bunch of accelerated electrons emitted from a plasma over the entire interaction time for various energy ranges. In all the figures, the azimuth angle φ is measured from the z axis, and the polar angle θ is counted from the direction of laser pulse propagation (x axis). Noticeable is the strong asymmetry of the distribution along the y and z axes. This asymmetry arises due to the linear polarisation of the laser pulse in the xy plane, which leads to a larger value of the transverse momentum in the y direction under the action of the electric laser field.

Goers et al. [3] measured the angular spread of electrons only across the direction of the laser pulse polarisation, where this value is much smaller than that in the direction of polarisation. The effective solid angle, determined by the width of the angular distribution only in the measured direction (the spectrum of accelerated electrons was normalised to this angle in [3]), was noticeably smaller than the solid angle found in our calculations taking into account the asymmetry of the emission of accelerated electrons. This circumstance determines the coefficient, by which the simulated spectrum of the emitted electrons is multiplied (Fig. 15). The effective temperature of accelerated electrons (the slope of their spectrum in Fig. 15) obtained from 3D PIC simulations well agrees with that found experimentally [3], which indicates the adequacy of the numerical analysis of the available experimental data.

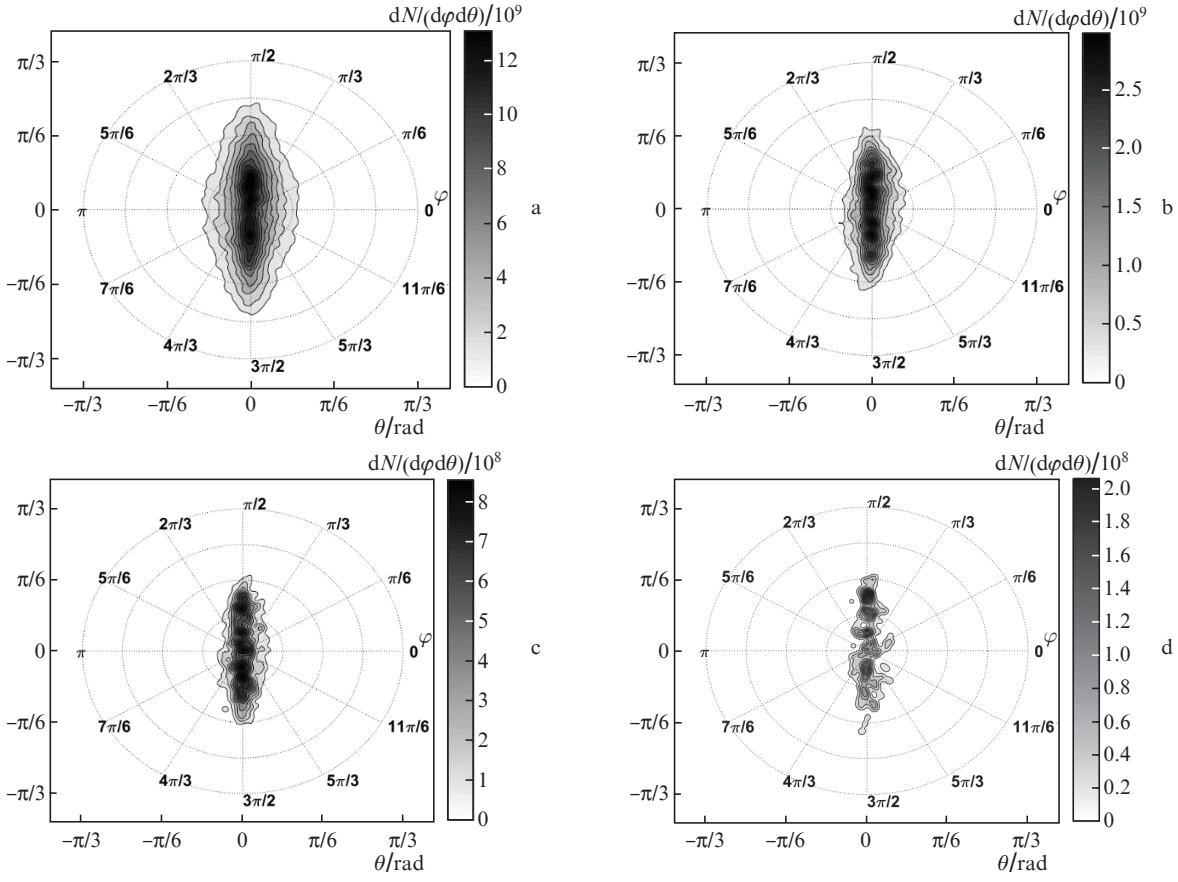

Figure 16. Distributions of electrons with energies above (a) 2, (b) 5, (c) 7 and (d) 9 MeV over the polar and azimuth angles [dN/(dφdθ)].

6. Conclusions

Using 3D PIC simulation, we have investigated the interaction of a subterawatt laser pulse with a nonuniform gas jet plasma. We have determined the conditions for the occurrence and characteristics of the processes of laser pulse self-focusing and self-modulation. The efficient generation of a wake plasma wave by a laser pulse is demonstrated under conditions when the pulse power exceeds the critical power for relativistic self-focusing, determined by the local plasma electron concentration. The parameters (amplitude and phase velocity) of a wake plasma wave generated in a nonuniform plasma in the self-modulation regime of a laser pulse are studied. Due to a decrease in the phase velocity of the wake wave and an increase in its amplitude during laser pulse self-modulation and self-focusing, as well as due to the contribution of linear effects of plasma concentration nonuniformity to a decrease in the wake wave phase velocity, the background plasma electrons are trapped and further accelerated in the wake field. We have determined the energy and angular characteristics of accelerated electrons. It is shown that when the acceleration region of electrons is limited to the length of their dephasing, the spectrum of accelerated electrons is characterised by the formation of a quasi-monoenergetic electron bunch with an energy of ~ 9 MeV and a charge of ~ 30 pC (for the considered parameters of the laser and plasma). The effective temperature of the accelerated electrons and their angular distribution, obtained by 3D PIC simulation, are in good agreement with those determined in the experiment.

Acknowledgements. This work was supported by the Presidium of the Russian Academy of Sciences (Fundamental Research Programme 'Extreme Light Fields and Their Interaction with Matter') and the Russian Foundation for Basic Research (Grant No. 19-02-00908).

The authors thank A. A. Golovanov for discussing the role of nonlinear effects of plasma nonuniformity in the process of decreasing the wake wave phase velocity.

References

1. Leemans W.P. et al. *Phys. Rev. Lett.*, **113**, 245002 (2014).
2. He Z.-H., Hou B., Nees J.A., Easter J.H., Faure J., Krushelnick K., Thomas A.G.R. *New J. Phys.*, **15**, 053016 (2013).
3. Goers A.J., Feder G.A., Miao B., Salehi F., Wahlstrand J.K., Milchberg H.M. *Phys. Rev. Lett.*, **115**, 194802 (2015).
4. Pugachev L.P., Andreev N.E., Levashov P.R., Malkov Yu.A., Stepanov A.N., Yashunin D.A. *Fiz. Plazmy*, **41** (7), 588 (2015).
5. Malkov Yu.A., Stepanov A.N., Yashunin D.A., Pugachev L.P., Levashov P.R., Andreev N.E., Andreev A.A. *Quantum Electron.*, **43** (3), 226 (2013) [*Kvantovaya Elektron.*, **43** (3), 226 (2013)].
6. Pugachev L.P., Popov V.S., Andreev N.E. *J. Phys.: Conf. Ser.*, **774**, 012106 (2016).
7. Andreev N.E., Gorbunov L.M., Kirsanov V.I., Pogosova A.A., Ramazashvili R.R. *JETP Lett.*, **55**, 509 (1992) [*Pis'ma Zh. Eksp. Teor. Fiz.*, **55**, 551 (1992)].
8. Pukhov A.J. *Plasma Phys.*, **61**, 425 (1999).
9. Popov V.S., Pugachev L.P., Andreev N.E. *J. Phys.: Conf. Ser.*, **1147**, 012078 (2019).
10. Gorbunov L.M., Kirsanov V.I. *Sov. Phys. JETP*, **66**, 290 (1987) [*Zh. Eksp. Teor. Fiz.*, **66**, 290 (1987)].
11. Andreev N.E., Kirsanov V.I., Gorbunov L.M., Sakharov A.S. *IEEE Transact. Plasma Sci.*, **24** (2), 363 (1996).